Multispectral Data Fusion for Robotic Reconnaissance and Mapping

Petra Kocmanova[1], Ludek Zalud[2], Frantisek Burian[2] and Tomas Jilek[2]
[1]*Institute of Geodesy, Brno University of Technology, Veveri 331/95, Brno, Czech Republic*
[2]*CEITEC, Brno University of Technology, Technicka 3082/12, Brno, Czech Republic*

Keywords: Data Fusion, Sensory Head, Range Camera, CCD Camera, Thermal Imager.

Abstract: The aim of the paper is to describe the data-fusion from optical sensors for mobile robotics reconnaissance and mapping. Data are acquired by stereo pair of CCD cameras, stereo pair of thermal imagers, and TOF (time-of-flight) camera. The fusion is realized by means of spatial data from a TOF camera to ensure ”natural” representation of a robot’s environment; thus, the thermal and CCD camera data are comprised in one stereo image presented to a binocular, head-mounted display. The data acquisition is performed using a sensor head, which is placed on an Orpheus-X3 robot; both the head and the robot were developed by our working group. After the geometrical calibration of each sensor, the positions of the sensors in 6DOFs are computed. The corresponding data from the CCD camera and the thermal imager are subsequently determined via homogeneous and perspective transformations. The result consists in an image containing aligned data from the CCD camera and the thermal imager for each eye. TOF camera calibration and its impact to the precision of fusion is described. Although the fusion is used for two different tasks – automatic environment mapping and visual telepresence, the utilised calibration and fusion algorithms are, in principle, the same.

1 INTRODUCTION

The described calibration and data-fusion algorithms may be used for two purposes: visual telepresence (remote control) under extremely wide variety of visual conditions, like fog, smoke, darkness, etc., and for multispectral autonomous digital mapping of the robot’s environment.

The method uses a combination of „classical“ cameras working in visible spectrum with thermal imagers working in 7-14um spectrum. Each of them has certain advantages and disadvantages.

Modern visible-spectrum cameras offer a very good overview of the situation with high resolution. Their image representation is the most intuitive for the operator. On the other hand the dynamic range of them is much lower than the one of a human eye. They also do not work in complete darkness, cannot see through fog or smoke.

Thermal imagers became widely available during the last couple years, when their price was reduced significantly. The main advantages - they can percept in fog, at least for short distances, they are also almost unaffected by visible light, so it does not matter how the scene is illuminated (complete darkness, point light sources, …). The main disadvantages – they offer significantly lower pixel resolution comparing to standard cameras, they are still significantly more expensive and the image offered is not so intuitive to the operator, since it basically corresponds to temperatures of the objects.

So it seems valuable to combine these two

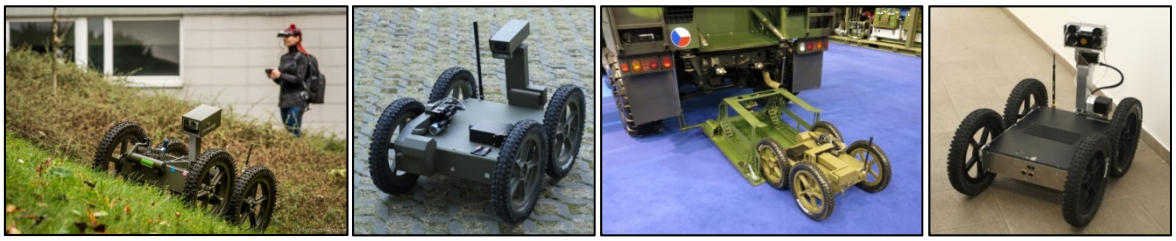

Figure 1: Orpheus robots (from left) – Orpheus Hope, Oprheus-AC2, Orpheus-AC2, Orpheus-X3.

Kocmanova P., Zalud L., Burian F. and Jilek T..
Multispectral Data Fusion for Robotic Reconnaissance and Mapping.
DOI: 10.5220/0005060504590466
In *Proceedings of the 11th International Conference on Informatics in Control, Automation and Robotics* (ICINCO-2014), pages 459-466
ISBN: 978-989-758-040-6

imagers into one image. Nowadays several companies provide combined CCD – thermal imagers, but their approach is simplistic – the images are only geometrically aligned, so because of parallax the images do not correspond exactly for most cases. Furthermore the used CCD cameras are typically of low quality and with limited field of view. So these solutions are not appropriate for telepresence in rescue robotics.

The technique was studied by our team in the past (Zalud, 2005), but as the sensory prices decreased and TOF cameras matured, the technique now may be done more advanced. In this article we introduce a technique for visual spectrum data and thermal imager data alignment with help of data from TOF camera. The TOF camera measures a distance of an object, while corresponding pixels are found on color camera and thermal imager. Each of the sensors has to be calibrated for geometrical errors, mutual position and orientation is found and used to make the correspondence calibrations.

This is done for two stereo-pairs of cameras, so the resulting image may be presented to head-mounted display with stereovision support, so the operator has a very good spatial representation of the surrounding under any visibility conditions.

It has to be pointed out the sensors on the sensory head will not be used only for this technique, in parallel we also develop SLAM technique with similar texture-mapping algorithms.

2 HARDWARE

2.1 Orpheus-X3

The Orpheus-X3 is an experimental reconnaissance robot based on the Orpheus-AC2 model made by our team to facilitate the measurement of chemical and biological contamination or radioactivity for military purposes (Fig. 1). The Orpheus-X3 offers the same drive configuration as its predecessor, namely the four extremely precise AC motors with harmonic gears directly mechanically coupled to the wheels; this configuration makes the robot very effective in hard terrain and enables it to achieve the maximum speed of 15 km/h. The main difference consists in the chassis, which is not designed as completely waterproof but consists of a series of aluminum plates mounted on a steel frame of welded L-profiles. This modular structural concept makes the robot markedly more versatile, which is a very important aspect in a robot made primarily for research activities. Furthermore, the device is equipped with a 3DOF manipulator for the sensory head. The manipulator, again, comprises very powerful AC motors combined with extremely precise, low backlash harmonic drive gearboxes by the Spinea company. The presence of such precise gearboxes can be substantiated by several reasons, mainly by the fact that the robot will be used not only for telepresence but also for mobile mapping and SLAM. As currently planned, the robot's only proximity sensor will be the TOF camera placed on the sensory head.

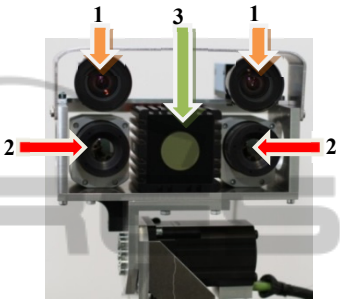

Figure 2: The sensory head. 1 – the tricolor CCD cameras, 2 – the thermal imagers, 3 – the TOF camera.

2.1.1 Sensory Head

The sensory head containing five optical sensors is shown in Fig. 2.

- Two tricolor CCD cameras (see 1 in Fig. 2). TheImagingSource DFK23G445 with 1280x960 pixels resolution, max refresh rate 30Hz, and GiGe Ethernet protocol. A Computar 5mm 1:1.4 lens is used.
- Two thermal Imagers (see 2 in Fig. 2). MicroEpsilon TIM 450 with a wide lens, 382x288 pixels resolution, temperature resolution of 0.08K, a USB output.
- One TOF camera (see 3 in Fig. 2). A Mesa Imaging SR4000 with the range of 10m, 176x144 pixels resolution, an Ethernet output. The field of view is 56˚(h) x 69˚(v).

From the preceding text we can conclude, the fields-of-view (FOVs) of the sensors are similar. The largest FOV captures TOF camera, which is required for simultaneous use of stereovision and thermal stereovision. The main disadvantage of the used TOF camera is its low number of pixels (spatial resolution). In relation to the CCD cameras is about 10 times lower in one axis and in relation to thermal imagers, it is 2 times lower.

3 SENSOR CALIBRATION PROCEDURE

The reasons for the sensory head calibration are following:

- Simultaneous use of all five sensors leads to necessity of determination translations and rotations among cameras.
- Absolute range precision guaranteed by the manufacturer for range camera is ± 15 mm, but only for the central 11 × 11 pixels. According to our experience, range measurement is less precise - for details see (Kocmanova, 2013)
- Temperature shift in color-coded thermal images (about 1.5K) must be resolved for simultaneous use of 2 thermal imagers.

With respect to the previous description, calibration of the sensory head consists of the following parts (see Fig. 3): range calibration, temperature calibration, calibration of intrinsic and extrinsic parameters.

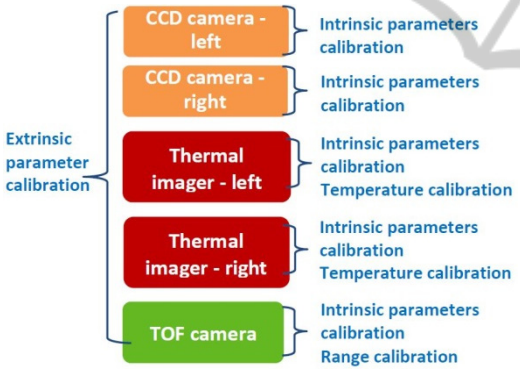

Figure 3: Calibration scheme for all sensors.

3.1 Range Calibration

Range calibration of the TOF camera is detailed described in (Kocmanova, 2013). Improvement of range accuracy is evident from Fig. 4. Range accuracy was tested in 4 regions (see Fig. 5) that are defined by manufacturer (SR4000, 2011).

3.2 Temperature Calibration

The microEpsilon TIM 450 low quality thermal imagers were used for this application. The main reason for this was the low price and very small dimensions. Although the temperature resolution (0.08K according to the datasheet) is relatively sufficient, the absolute precision of 2K can be defined as poor.

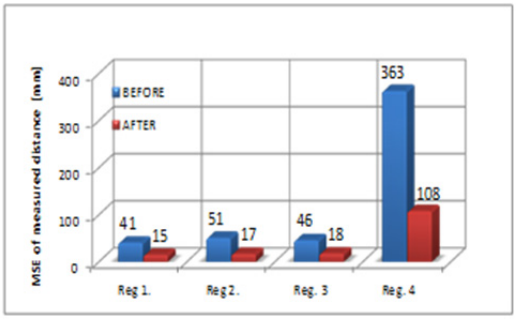

Figure 4: MSE of measured distance for all regions of TOF camera before and after calibration.

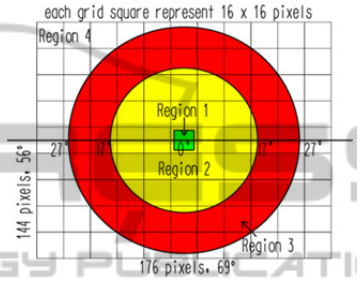

Figure 5: Image division of TOF camera into the region by accuracy.

In our application, we use two identical thermal imagers for stereovision. The temperatures are "expressed" by colour-coding. In most cases, the range of colors displayed is quite small (couple of K). To provide the most relevant data to the operator, it is important to use the narrowest temperature range possible, because the more different are the colors representing the nearby temperatures, the better the visual perception is. But as it was already mentioned, the temperature shift between the two cameras may be - and indeed often is during the first 30 minutes of operation - in the order of Kelvins. This may cause unwanted color shift between the left and right images (Fig. 6).

Figure 6: The temperature shift in the color-coded left and right thermal images provided by the TIM450 cameras: the calculated temperature shift is 1.5K. The grayscale coding (upper row); the thermal-red coding (bottom row).

The algorithm to solve this problem is as follows: A temperature histogram of the left and right images is made, and the cross-correlation (Eq. 1) function is calculated. The maximum on the resulting function corresponds to the actual mutual temperature shift between the cameras, and therefore we then shift the temperatures in one of the matrices.

$$cc(k) = \sum_{i=0}^{hc} (hist\_l(i) * hist\_r(k+i)) \quad (1)$$

where *hist_l* and *hist_r* are the temperature discrete histograms of the left or right thermal image respectively, and *hc* is the histogram dimension.

3.3 Calibration of Intrinsic and Extrinsic Parameters

An interesting problem was to find a material from that a pattern would be clearly identifiable in the images of all sensors. For opaque body, the sum of surface reflectivity and emissivity equals to 1 (Bartl). To create a calibration plate it is necessary to select two materials with significantly different emissivity (i.e. also reflectivity). If the emissivity of both materials isn´t sufficiently different, it is possible to increase the contrast between materials by heating one of them.

There are various options to find sufficiently contract materials. In (Luhmann, 2010) authors create plane test field that consists of wooden board with 57 small lamps that warm up when switched on and test field based on a metal surface with coded and uncoded circle target points created using self-adhesive foil. In (X.Ju, 2005) plane with heated circle target was used for calibration of thermal imager and color camera stereo pair, and in (Prakash, 2006) a pair of thermal imagers was calibrated with checker-board pattern heated by a flood lamp.

We proposed checkerboar calibration plate. First version of calibration was from aluminum plate (low emissivity, high reflectivity) and self-adhesive foil (high emissivity, low reflectivity). This board had a problem with high reflectivity of aluminum base.

Second version was aluminum plate with laser-cut pattern coated by anodizing behind that was aluminum plate chipboard covered by black matte foil. Final version is 2mm thin laser-cut aluminum plate with active heating (see Fig. 7)

Calibration of intrinsic and extrinsic parameters is based on (Zhang, 1999) and is realized as follows: the first step consisted in edge extraction, the second was the initial calibration of intrinsic and extrinsic parameters, and the last stage of the calculation included nonlinear optimization (which minimizes the sum of the squares of the re-projection errors including the determination of distortion). The mathematical model is detailed described in (Zalud, 2013, SSRR).

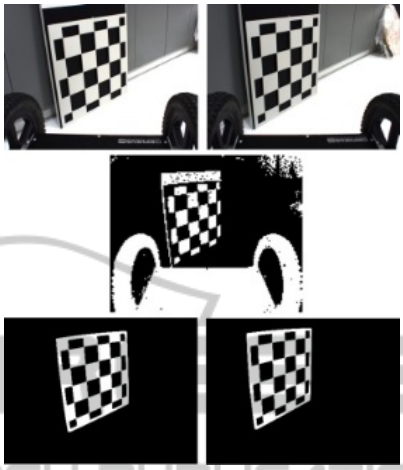

Figure 7: The calibration target: the left and right CCD cameras (up), the TOF camera intensity image (center), the left and right thermal imagers (down) camera.

4 DATA FUSION PROCESS

Image transformations are applied for data fusion. The range measurements of the TOF camera can be displayed into images of CCD cameras and thermal imagers using spatial coordinates. The procedure is outlined in the diagram below (see Fig. 8). The input data include the range measurement, the image coordinates of all sensors, and the results of the previous calibration.

The spatial coordinates *X, Y, Z* are computed according to Eq. 2 and 3, where *d* is the measured distance, x_c, y_c are the calibrated TOF image coordinates, and *f* is the focal length of the TOF camera. The homogeneous transformation is determined by Eq. 4, where $R_{[3\times3]}$ is the rotational matrix, $t_{[3\times1]}$ is the translation vector, and *X′, Y′, Z′* are the spatial coordinates of the second sensor. The image coordinates of the TOF camera in the next frame x_c', y_c' are computed according to perspective projection (see Eq. 5), where *f′* is the focal length of the second sensor.

$$Z = d\cos\left(\arctan\left(\frac{y_c}{\sqrt{f^2 + x_c^2}}\right)\right)\cos\left(\arctan\left(\frac{x_c}{f}\right)\right) \quad (2)$$

$$X = \frac{Zx_c}{f}, Y = \frac{Zy_c}{f} \quad (3)$$

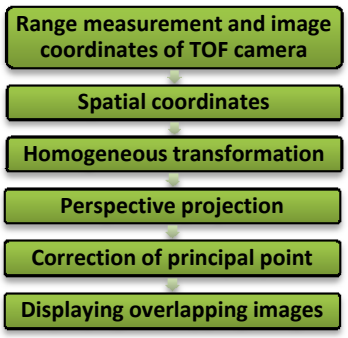

Figure 8: Image transformation scheme.

$$\begin{bmatrix} X' \\ Y' \\ Z' \\ 1 \end{bmatrix} = \begin{bmatrix} R & t \\ 0 & 1 \end{bmatrix} \begin{bmatrix} X \\ Y \\ Z \\ 1 \end{bmatrix} \quad (4)$$

$$x_c' = \frac{f'X'}{Z'}, y_c' = \frac{f'Y'}{Z'} \quad (5)$$

According to the identical (ID) points of the TOF camera transformed into the frames of the CCD camera and the thermal imager, the thermal image can be displayed into the CCD image and vice versa.

The main objective of this paper is to calculate and verify the accuracy of heterogeneous sensor data fusion. We will focus on the weakest point of data fusion i.e. range camera.

4.1 Influence of Distance Error on Data Fusion Precision

The first investigated problem is influence of objective point accuracy (or more precisely range accuracy) on data fusion. Therefore, we determined pixel differences caused by TOF camera radial distance error for both CCD cameras and thermal imagers. We simulated distance error for 2 significant image points: point on optical axis of the TOF camera, point on the edge of the region 3 (see Fig. 5) lying on the x-axis. Measured distances in the region 4 have very low reliability, therefore this region isn´t considered. The range of the radial distance simulation is the same as detection range of TOF camera i.e. 0.1 – 10.0 m.

The effect of distance error is not significant for data fusion if transformed image coordinate differences (CCD cameras and thermal imagers) not exceed 0.5 pixel. For simulation we used values

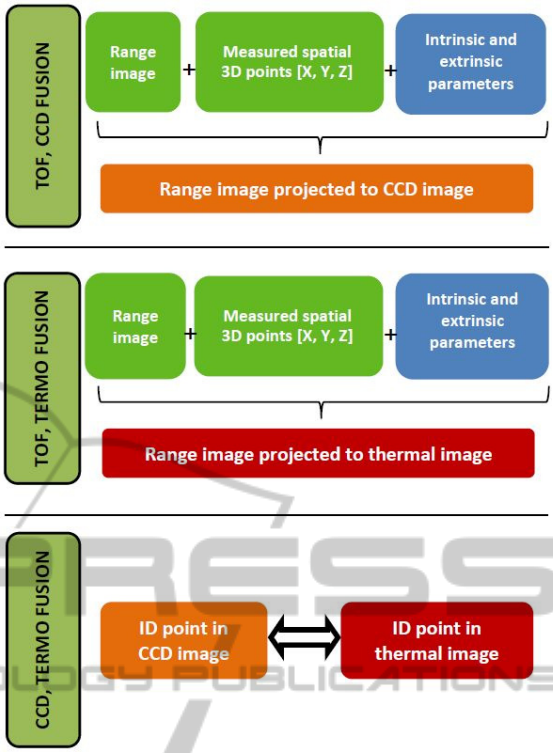

Figure 9: Scheme of data fusion: up – TOF and CCD data fusion; centre - TOF and thermal data fusion; down - CCD and thermal data fusion.

based on distance error from range calibration. It is also important to judge the usefulness and impact of the range calibration. Distance error before calibration 41 mm and after calibration 14 mm was used for point on optical axis (reg. 1). Analogously 46 mm and 18 mm for point on the edge of reg. 3.

Figs. 10, 11 and Tab. 1 show effect of pixel error in transformed images caused by distance error. Graphs for point on the edge of reg. 3 have the same character as Figs. 10 and 11. The numerical difference is apparent from Tab. 1. For point on the edge of reg. 3 are pixel error slightly higher than point on optical axis (reg. 1). Distance error is insignificant for radial distance greater than approximately 2.5 m for CCD cameras before range calibration and approximately 1.5 m for CCD cameras after range calibration. Analogously to thermal imagers, approximately 1.5 m before calibration and 1 m after calibration.

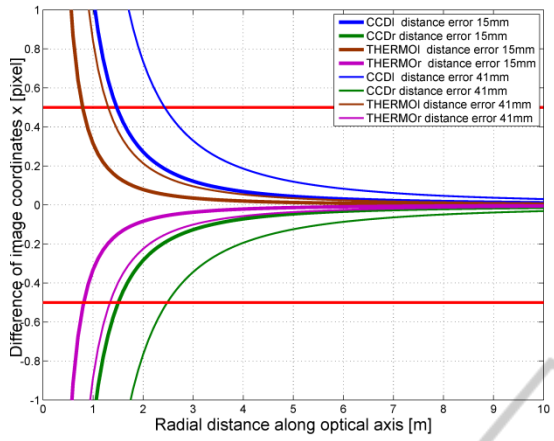

Figure 10: Image coordinate differences Δx caused by distance error for point on optical axis of TOF camera.

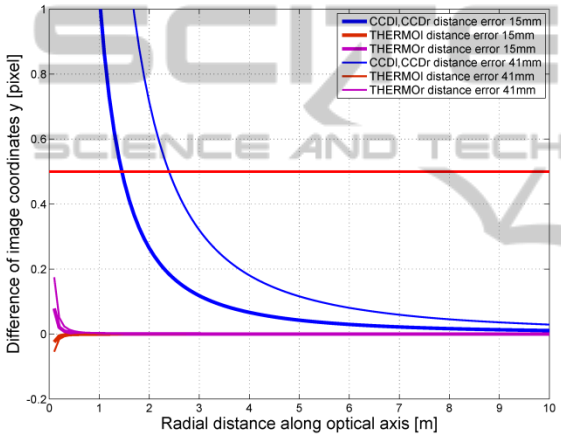

Figure 11: Image coordinate differences Δy caused by distance error for point on optical axis of TOF camera.

Table 1: Image Coordinate Differences 0.5 Pixel Cased By Distance Error.

	Distance error	Image coord.	Radial distance at that pixel error causes by distance error is 0.5 pixel [m]			
			CCDl	*CCDr*	*TH. l*	*TH. r*
Point on optical axis	***41 mm before calibration***	x	2.43	2.49	1.30	1.34
		y	2.40	2.40	–	–
	15 mm after calibration	x	1.48	1.51	0.79	0.81
		y	1.45	1.45	–	–
Point on the edge of reg. 3	***46 mm before calibration***	x	2.61	2.94	1.44	1.53
		y	2.64	2.64	–	–
	18 mm before calibration	x	1.64	1.84	0.90	0.97
		y	1.65	1.65	–	–

Influence of low resolution of TOF camera is the second investigated problem. The same 2 points and same distance range as in previous section are used for the simulation.

4.2 Influence of TOF Camera Low Resolution on Data Fusion Precision

Error 0.5 pixel in the image of TOF camera cause an error of image coordinate x for CCD cameras approximately 5 pixel (see Figs. 12, 14) and for thermal imagers approximately 1.5 pixel (see Figs. 12, 14).

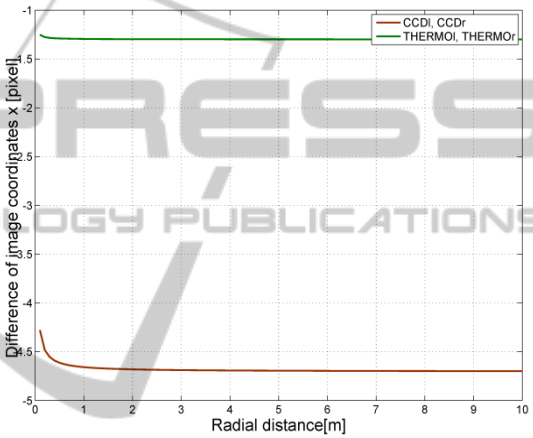

Figure 12: Image coordinate differences Δx caused by shift of TOF image coordinate x of 0.5 pixel for point on optical axis of TOF camera.

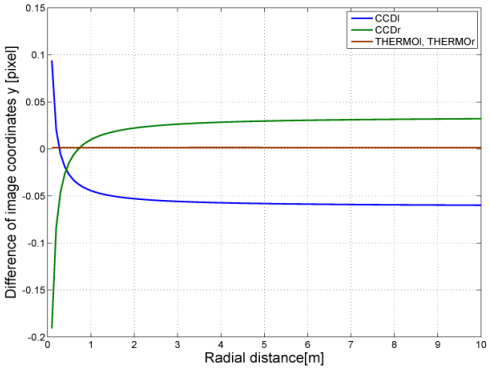

Figure 13: Image coordinate differences Δy caused by shift of TOF image coordinate x of 0.5 pixel for point on optical axis of TOF camera.

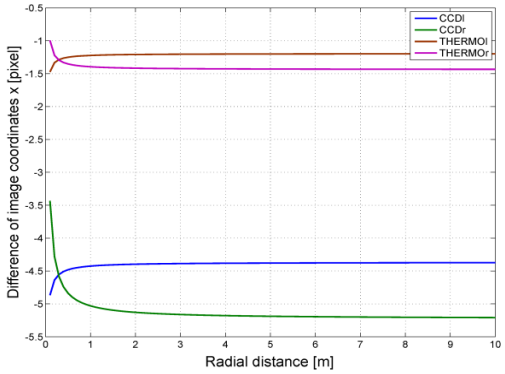

Figure 14: Image coordinate differences Δx caused by shift of TOF image coordinate x of 0.5 pixel for point on the edge of reg. 3.

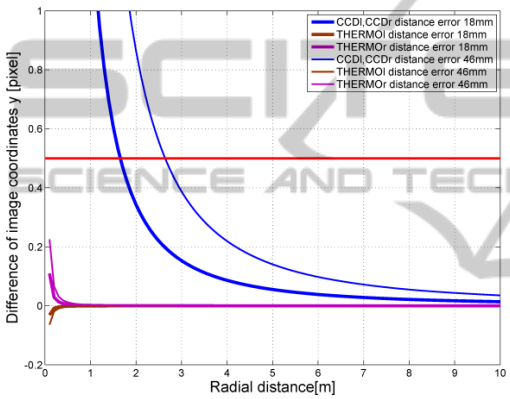

Figure 15: Image coordinate differences Δy caused by shift of TOF image coordinate x of 0.5 pixel for point on the edge of reg. 3.

Error of image coordinate y is insignificant for thermal imagers that are in the same height as TOF camera and for CCD cameras only for points near the optical axis of TOF camera (see Figs. 13 and 15). Influence of low resolution of TOF camera is significant for points remote from optical axis (see Fig. 13). Range calibration significantly improves precision of CCD image coordinate y in this case (see Fig. 15).

4.3 Influence of the TOF Image Radial Distance on Data Fusion Precision

The third simulated effect was the influence of the TOF camera image radial distance on data fusion precision. The simulation comprised the error of 0.5 pixel in the TOF camera image coordinates and the values of this error after the data fusion in images of the CCD cameras and thermal imagers depending on TOF image radial distance.

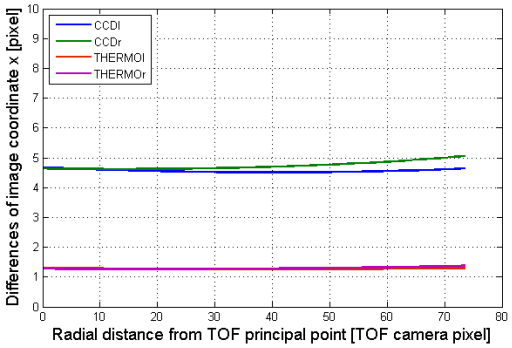

Figure 16: Image coordinate differences Δx caused by 0.5 TOF pixel error in dependence on the TOF image radial distance.

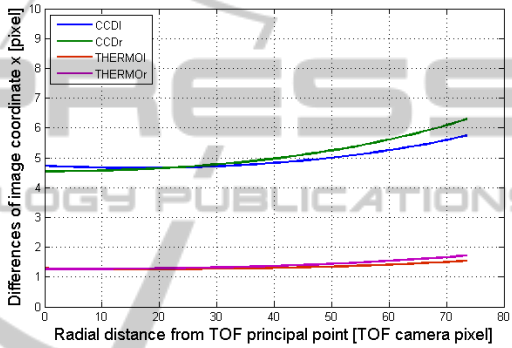

Figure 17: Image coordinate differences Δy caused by 0.5 TOF pixel error in dependence on the TOF image radial distance.

Different camera resolution values appear fully in this simulation. The error of 0.5 pixel in the TOF camera image causes, in the image coordinates x, y, the error of approximately 5 pixels for the CCD cameras and 1.5 pixels for the thermal imagers (see Fig. 16, 17). Furthermore, the influence of low resolution of the TOF camera slightly increases depending on the TOF camera radial distance.

5 CONCLUSION AND FUTURE WORK

Although the methods presented in this research report are sufficiently applicable, stable, and reliable (see Fig. 18), our research on the telepresence and mapping subsystem of CASSANDRA is still far from complete. The challenge we are currently facing is to facilitate seamless combination of visual telepresence and digital maps to form an augmented reality system. The system should be able to add map information to the "real-time" telepresence

image so that the operator could see data such as the temperatures through a robot that is not equipped with a thermal imager; furthermore, it should also facilitate the vision through or behind objects, and perform other operations.

The CASSANDRA system is obviously also intended to work outdoors, where other challenges are waiting. We have already integrated a Velodyne scanner as well as a high-precision RTK GNSS in one of our robots, and thus we can build also outdoor maps. We are currently working on several supporting systems for outdoor telepresence.

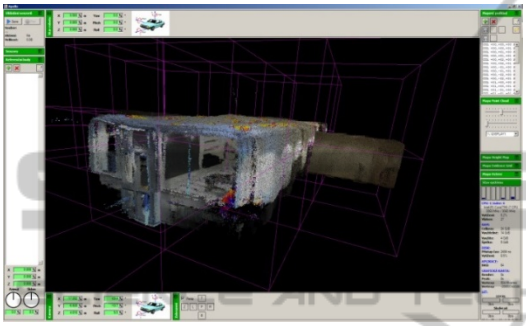

Figure 18: Octree multispectral map of interior with data-fusion.

ACKNOWLEDGEMENTS

This work was realised in CEITEC – Central European Institute of Technology with research infrastructure supported by the project CZ.1.05/1.1.00/02.0068 financed from European Regional Development Fund and by the Technology Agency of the Czech Republic under the project TE01020197 "Centre for Applied Cybernetics 3".

REFERENCES

P. Kocmanova and L. Zalud, “Spatial Calibration of TOF Camera, Thermal Imager and CCD Camera”. In: Mendel 2013: *19th International Conference on Soft Computing*. Brno: Brno University of Technology, Fakulty of Mechanical Engineering, 2013, s. 343-348. ISBN 978-80-214-4755-4.

SR4000 Data Sheet, MESA Imaging AG. Rev. 5.1, 2011.

J. Bartl and M. Baranek, “Emissivity of aluminium and its importance for radiometric measurement”. Measurement science review.

T. Luhmann, J. Ohm, J. Piechel and T. Roelfs, “Geometric Calibration of Thermographic Cameras”. In: *International Archives of Photogrammetry*, Remote Sensing and Spatial Information Sciences 2010, vol. XXXVIII, pp. 411-416.

X. Ju, J.-C. Nebel, J. P. Siebert, H. Gong, Y. Cai and J.-P. Chatard,” 3D thermography imaging standardization technique for inflammation diagnosis”. *Proceedings of the SPIE*. 2005, vol. 5640, pp. 266-273.

S. Prakash, P. Y. Lee and T. Caelli,” 3D Mapping of Surface Temperature Using Thermal Stereo”. 2006 *9th International Conference on Control, Automation, Robotics and Vision*. IEEE, 2006, pp. 1-4.

Z. Zhang,”Flexible camera calibration by viewing a plane from unknown orientations”. *Proceedings of the Seventh IEEE International Conference on Computer Vision*. IEEE, 1999, vol. 1, pp. 666-673.

L. Zalud and P. Kocmanova,”Fusion of Thermal Imaging and CCD Camera-based Data for Stereovision Visual Telepresence”.In: SSRR 2013: *11th IEEE International Symposium on Safety Security and Rescue Robotics*, pp.1-6.

L. Zalud, F. Burian, L. Kopecny, P. Kocmanova (2013). Remote Robotic Exploration of Contaminated and Dangerous Areas, *International Conference on Military Technologies*, pp 525-532, Brno, Czech Republic, ISBN 978-80-7231-917-6.

L. Zalud, (2005). ORPHEUS – Reconniaissance Teleoperated Robotic System. In: *16th IFAC World Congress*. pp. 1-6, Prague, Czech Republic.

D. Lichti, D.-Rouzaud: Surface-dependent 3D range camera self-calibration. In: *Proceedings of SPIE Three-Dimensional Imaging Metrology*, Vol. 7239, 2009, pp. 72390A-1-72390A-10.